UNDER-ICE BOUNDARY LAYER

M.G. McPhee, McPhee Research Company Naches, WA 98937, USA

James H. Morison
University of Washington, Applied physics Laboratory, Polar Science Center, 1013NE 40th street, Seattle, WA 98105, USA

doi:10.1006/rwos.2001.0146

Introduction

0001 Sea ice is in almost constant motion in response to wind, ocean currents, and forces transmitted within the ice cover itself, thus there is nearly always a zone of sheared flow between the ice and underlying, undisturbed ocean where turbulence transports momentum, heat, salt, and other contaminants vertically. The zone in which these turbulent fluxes occur, which can span from a few to hundreds of meters, is the under-ice boundary layer (UBL). This article describes general characteristics of the UBL, with emphasis on the physics of vertical turbulent transfer, specifically *turbulent mixing length* and eddy diffusivity. Extensive measurements of turbulence in the UBL, not available elsewhere, have not only made these ideas concrete, but have also provided quantitative guidance on how external forcing controls the efficiency of vertical exchange. Here we stress features that the UBL has in common with ocean boundary layers everywhere. The article on ice–ocean interaction emphasizes unique aspects of the interaction between sea ice and the ocean (Art. 3).

0002 While largely responsible for the relative paucity of oceanographic data from polar regions, sea ice also serves as an exceptionally stable platform, often moving with the maximum velocity in the water column. In effect, it provides a rotating geophysical laboratory with unique opportunities for directly measuring turbulent fluxes of momentum, heat, and salt at multiple levels in the oceanic boundary layer–measurements that are extremely difficult in the open ocean. Examples of important oceanographic boundary-layer processes first observed from sea ice include: (1) the Ekman spiral of velocity with depth; (2) Reynolds stress through the entire boundary layer, and its associated spiral with depth; (3) direct measurements of turbulent heat flux and salinity flux; (4) direct measurements of eddy viscosity and diffusivity in the ocean boundary layer; (5) the impact of surface buoyancy, both negative and positive, on boundary layer turbulence, and (6) internal wave drag ('dead water') as an important factor in the surface momentum and energy budgets.

0003 The UBL differs from temperate open ocean boundary layers by the absence of strong diurnal forcing and of high frequency, wind-driven surface waves. It thus lacks the near surface zone of intense turbulence and dissipation associated with wave breaking, and organized Langmuir circulation due to the nonlinear interaction between waves and currents (e.g., the interaction of Stokes drift with near surface vorticity). On the other hand, quasi-organized roll structures associated with sheared convective cells have been observed under freezing ice, and are apparently a ubiquitous feature of freezing leads and polynyas. Large inertial-period oscillations in UBL horizontal velocity are observed routinely, especially in summer when the ice pack is relaxed. The annual cycle of buoyancy flux from freezing and melting mimics in some respects the diurnal cycle of heating and cooling, as well as the annual evolution of temperate ocean boundary layers. The range of surface forcing, with observations of surface stress ranging up to 1 Pa, and buoyancy flux magnitudes as high as $10^{-6}\,\mathrm{W\,kg^{-1}}$, is comparable to that encountered in open oceans. All these factors suggest that similarities between the UBL and the open ocean boundary layer far outweigh the differences.

History and Basic Concepts

Rotational Physics and the Ekman Layer

0004 From 1893 to 1896, the Norwegian research vessel *Fram* drifted with the Arctic pack ice north of Eurasia in one of the most productive oceanographic cruises ever conducted. Among other important discoveries was the observation by Fridtjof Nansen, the great scientist–explorer–statesman, that the drift was consistently to the right of the surface wind. Nansen surmised that this effect arose from the differential acceleration in a rotating reference frame (the earth) on the sheared turbulent flow beneath the ice, and interested the young German scientist, V.W. Ekman, in the problem. Ekman discovered an elegantly simple solution to the coupled differential equations describing the steady-state boundary layer, which exhibited attenuated circular

rotation with depth (spirals) in both velocity and stress (momentum flux). The solution includes a constant phase difference between velocity and stress, resulting in a 45° clockwise deflection of surface velocity with respect to surface stress in the Northern Hemisphere, roughly comparable to the 20–40° deflection Nansen observed. In his classic 1905 paper, Ekman extended his findings with remarkable insight to predict *inertial oscillations*, large circular currents superimposed on the mean current, and even derived credible estimates of eddy viscosity in the ocean from surface-drift-to-wind-speed ratios. Ekman postulated the eddy viscosity should vary as the square of the surface wind speed, with kinematic values of order $0.04\,m^2\,s^{-1}$ for typical wind speeds of $10\,m\,s^{-1}$.

0005 After nearly a century, it is tempting to dismiss Ekman's solution as not adequately accounting for vertical variation of eddy viscosity in the boundary layer. Surface (ice) velocity, for example, is strongly influenced by a zone of intense shear near the ice–ocean interface where eddy viscosity varies linearly with distance from the ice. For typical under-ice conditions, this approximately halves the angle between interfacial stress and velocity and significantly increases the ratio of surface speed to surface stress. The Ekman approach also ignores potentially important effects from density gradients in the water column, or from buoyancy flux at the interface. Nevertheless, measurements from the UBL show that with slight modification, Ekman theory does indeed provide a very useful first-order description of turbulent stress in the UBL. Turbulent stress is not much affected by either variation in eddy viscosity in the near surface layer (across which the stress magnitude varies by only about 10%), or by horizontal gradients in density of the boundary layer ('thermal wind'). Both can have large impact on the mean velocity profile.

0006 The Ekman solution for turbulent stress is derived as follows. Using modern notation, the equations of motion in a noninertial reference frame rotating with the earth include an apparent acceleration resulting in the Coriolis force, with horizontal vector component $\rho f\boldsymbol{k}\times\boldsymbol{V}$, where ρ is density, $\boldsymbol{V}$ is the horizontal velocity vector, $\boldsymbol{k}$ is the vertical unit vector, and f is the Coriolis parameter (positive in the Northern Hemisphere). Ekman postulated that *eddy viscosity*, K, which behaves similarly to molecular viscosity but is several orders of magnitude larger, relates stress to velocity shear: $\hat{\tau} = K\partial\boldsymbol{V}/\partial z$ where $\hat{\tau}$ is a traction vector combining the horizontal components of stress in the water. Expressing horizontal vectors as complex numbers, e.g., $\boldsymbol{V} = u + iv$, the steady-state, horizontally homogeneous equation for horizontal velocity in an otherwise quiescent ocean forced by stress at the surface is then given by:

$$if\boldsymbol{V} = K\frac{\partial^2\boldsymbol{V}}{\partial z^2} \qquad [1]$$

Implicit in eqn [1] is that K does not vary with depth, so differentiation of eqn [1] with respect to z and substituting $\hat{\tau}/K$ for $\partial\boldsymbol{V}/\partial z$ yields a second-order differential equation for $\hat{\tau}$ subject to boundary conditions that $\hat{\tau}$ vanish at depth and that it match the applied interfacial stress, $\hat{\tau}_0$ at $z = 0$.

The solution is simply: 0007

$$\hat{\tau}(z) = \hat{\tau}_0 e^{\hat{\delta}z} \qquad [2]$$

where $\hat{\delta} = (f/|f|)(if/K)^{1/2}$ is a complex extinction coefficient that both attenuates and rotates stress with increasing depth, clockwise in the Northern Hemisphere, counterclockwise in the Southern Hemisphere.

0008 The practical differences between Ekman spirals in velocity and stress are illustrated by measurements of mean velocity and Reynolds stress during a period of rapid ice drift at Ice Station Weddell near 65°S, 50°W (**Figure 1**). The mean current in a reference frame drifting with the ice velocity (i.e., the negative of the dashed vector labeled 'Bot' in **Figure 1A**) shows the characteristic leftward turning with depth, but also includes a region of strong shear between 4 m and the ice–ocean interface, as well as an apparent eastward geostrophic current of several centimeters per second. The last may include its own vertical shear unrelated to UBL dynamics. None of these complicating factors has much impact on the Reynolds stress (**Figure 1B**), which shows (in a general sense) the depth attenuation and rotation predicted by a simple complex exponential (2) with vertically invariant eddy viscosity. The latter derives from a similarity based value for K, proportional to $|\hat{\tau}_0/f|$, with a magnitude of about $0.02\,m^2\,s^{-1}$. Since the interfacial stress is approximately proportional to wind speed squared, this is indeed similar to Ekman's development,[1] with the magnitude implied by the observations within a factor of about two of Ekman's prediction. Although the profile of **Figure 1(B)** is especially 'clean,' numerous other examples of spirals in Reynolds stress profiles exist from under-ice measurements, most consistent with the neutral scaling implied by $K \propto |\hat{\tau}_0/f|$. Thus despite its simplicity, the Ekman approach provides a remarkably accurate account of momentum flux in the UBL for many commonly encountered situations. It is a relatively minor step to adjust the surface velocity

to account for the variable K surface layer. Done properly, this leads to a *Rossby similarity* drag formulation.

Buoyancy Flux and the Seasonal Cycle

0009 The other major factor by which the under-ice boundary layer interacts with the ice cover and atmosphere is the annual cycle of mixed layer temperature, salinity, and depth. During summer, the mixed layer warms, freshens, and shoals, to be followed during and after freezeup, by cooling (to freezing), salination, and deepening. Although this cycle emulates in many ways the annual cycle of temperate mixed layers, a major distinction is that buoyancy is controlled mainly by salinity rather than temperature (the thermal expansion coefficient decreases rapidly as T approaches freezing, whereas the saline contraction coefficient remains relatively constant), thus freezing or melting at the ice–ocean interface is the main source of buoyancy flux for the UBL.

0010 In the perennial pack of the Arctic, heat absorbed in the upper ocean through summer leads, melt ponds, and thin ice contributes to bottom melting and is an important part of both the ice mass balance and the total summer buoyancy increase for the UBL. Away from the continental shelves and ice margins, heat exchange with the deep ocean tends to be small, limited by the cold halocline that separates water of Atlantic origin from the surface. In the eastern Arctic, the marginal ice zone of Fram Strait, and in the vast seasonal sea ice zone surrounding the Antarctic continent, the UBL interacts directly with warmer deep ocean, and oceanic heat mixed into the boundary layer from below often controls the ice mass balance, and exerts major influence on overall ocean stability.

0011 Buoyancy plays a major role in these exchange processes and is not adequately represented by treating eddy viscosity as dependent solely on surface stress. Most of the UBL research in recent years has been devoted to understanding how buoyancy influences turbulent fluxes.

Turbulence in the Under-ice Boundary Layer

Reynolds Flux

0012 When ice is in motion relative to the underlying water, there is a net flux of momentum in the underlying boundary layer, most of which is carried by turbulent fluctuations arising from relatively small, chaotic instabilities in the flow, motions which will also induce fluxes of scalar properties (e.g., T, S) if a mean gradient in the property exists. The turbulent transport process is best demonstrated by considering the advective part of the material derivative. Consider, for example, the simplest form of the heat equation: horizontally homogeneous, with no internal sources or sinks of heat. In an Eulerian reference frame, this reduces to a simple balance between the material derivative of temperature and the vertical gradient of the molecular heat diffusion

$$\frac{dT}{dt} = \frac{\partial T}{\partial t} + \boldsymbol{u}\cdot\nabla T = \frac{\partial}{\partial z}\left(\nu_T \frac{\partial T}{\partial z}\right) \qquad [3]$$

where ν_T is the molecular thermal diffusivity. Turbulent flux of temperature variations arises from the advective term, $\boldsymbol{u}\cdot\nabla T$. If velocity and temperature are expressed as the sum of mean and turbulent (fluctuating) parts: $\boldsymbol{u} = \bar{\boldsymbol{U}} + \boldsymbol{u}'$ and $T = \bar{T} + T'$, and the flow is incompressible and horizontally homogeneous with no mean vertical velocity,

$$\boldsymbol{u}\cdot\nabla T = \frac{\partial}{\partial z}\langle w'T'\rangle \qquad [4]$$

Normally this term completely dominates the molecular flux and eqn [3] is approximated by

$$\frac{\partial \bar{T}}{\partial t} = \frac{\partial}{\partial z}\langle w'T'\rangle \qquad [5]$$

In a strict sense, the angle brackets represent an ensemble Reynolds average over many independent realizations of the flow, but for practical applications it is assumed that the large-scale, 'mean' properties of the flow and its turbulent fluctuations respond in different and separable wavenumber bands (so that the local time derivative in eqn [5] has meaning), and that a suitable average in time is representative of the Reynolds flux.

A similar analysis of $d\boldsymbol{u}/dt$ leads to the divergence 0013
of the Reynolds stress tensor formed from the velocity covariance matrix of the three fluctuating velocity components. Under the same simplifications as above, the advective term in the mean horizontal velocity equation becomes

$$\frac{\partial}{\partial z}(\langle u'w'\rangle + i\langle v'w'\rangle)$$

where the horizontal vector quantity $\tau = \langle u'w'\rangle + i\langle v'w'\rangle$ is traditionally called Reynolds stress. A second important turbulence property associated with the Reynolds stress tensor is its trace

$$q^2 = \langle u'u' \rangle + \langle v'v' \rangle + \langle w'w' \rangle \qquad [6]$$

which is twice the *turbulent kinetic energy* (TKE) per unit mass.

0014 The connection between turbulence and eddy viscosity becomes apparent when the horizontal velocity equation is written with the simplifying (but often reasonable) assumptions of horizontal homogeneity, no mean vertical velocity, and negligible impact of molecular viscosity:

$$\frac{\partial \boldsymbol{V}}{\partial t} + if\boldsymbol{V} = \frac{\partial}{\partial z}(\langle u'w' \rangle + i\langle v'w' \rangle) = \frac{\partial}{\partial z}\left(u_\tau \lambda \frac{\partial \boldsymbol{V}}{\partial z}\right) \qquad [7]$$

The last term in eqn [7] represents the *mixing-length hypothesis*, essentially a scaling argument that Reynolds stress is uniquely related to the mean velocity shear by the product of velocity and length scales characterizing the largest, energy-containing eddies in the flow. Eddy viscosity is $K = u_\tau \lambda$. The steady version of eqn [7] differs from eqn [1] in that K may depend on z and remains within the scope of the outer derivative.

Scales of Turbulence

0015 A reasonable choice for the turbulence velocity scale (u_τ) is the *friction speed* $u_* = \sqrt{(\hat{\tau})}$.. In exceptional cases where destabilizing buoyancy flux ($\langle w'b' \rangle = (g/\rho)\langle \rho' w' \rangle$) from rapid freezing is the main source of turbulence, a more appropriate choice is the convective scale velocity $w_* = (\lambda |\langle w'b' \rangle_0|)^{1/3}$ where λ is the length scale of the dominant eddies. An alternative scale is q given by eqn [6]; however, observations in the UBL show the ratio q/u_* to be relatively constant (~ 3) in shear-dominated flows; the distinction may therefore be academic until a clear connection between q and w_* is demonstrated.

0016 Mixing length is the distance over which the 'energy-containing' eddies are effective at diffusing momentum. Several observational studies in the UBL have shown a robust relationship between a length scale λ_{peak} inversely proportional to the wavenumber at the maximum of the weighted spectrum of vertical velocity, and λ inferred by other methods. Since the spectrum of vertical velocity is relatively easy to measure, λ_{peak} provides a useful proxy for estimating λ simultaneously at several levels in the UBL.

0017 A diagram of governing turbulence scales in the UBL is presented in **Figure 2**, developed by combining simple boundary-layer similarity theory with numerous observations from drifting sea ice ranging from the marginal ice zone of the Greenland Sea, to the central Arctic ocean under thick ice and at the edges of freezing leads, and in the Weddell Sea. **Figure 2(A)** shows neutral stratification in the bulk of the UBL, when surface buoyancy flux (melt rate) is too small to have appreciable impact on turbulence. This is a common condition for perennial pack ice, which grows or melts slowly most of the year. Working from the interface down, mixing length increases approximately linearly with depth through the *surface layer*, until it reaches a limiting value proportional to the planetary length scale $\lambda_{max} = \Lambda_* u_{*0}/f$, where $\Lambda_* \sim 0.03$. Usually, the surface layer extends 5 m orless. From there the mixing length holds relatively constant through the extent of the Ekman (or outer) part of the UBL, to the depth of the pycnocline (typically 35–50 m in the western Arctic; 75–150 m in the Weddell Sea). If the neutral layer is very deep, stress decreases more or less exponentially, following approximately the Ekman solution (see the discussion of **Figure 3B** below); however, if the pycnocline is shallow, a finite stress will exist at z_p (indicated in **Figure 2** by u_{*p}) instigating upward mixing of pycnocline water with associated buoyancy flux, $\langle w'b' \rangle_p$. Mixing length in the highly stratified fluid just below the mixed-layer–pycnocline interface is estimated from the *turbulent kinetic energy equation*, which is dominated by three terms: production of TKE by shear ($P_S = \hat{\tau} \cdot \partial \boldsymbol{U}/\partial z$), production by buoyancy ($P_b = -\langle w'b' \rangle$), and dissipation by molecular forces (ε). Relating stress and shear by the mixing-length hypothesis, the balance of TKE production with dissipation is

$$u_*^3/\lambda - \langle w'b' \rangle = \varepsilon \qquad [8]$$

The negative ratio of buoyancy production to shear production is the flux Richardson number:

$$-P_b/P_S = \frac{\lambda \langle w'b' \rangle}{u_*^3} = \frac{\lambda}{\kappa L} \qquad [9]$$

where $L = u_*^3/(\kappa \langle w'b' \rangle)$ is known as the Obukhov length. Studies of turbulence in stratified flows have shown that the ratio [9] does not exceed a limiting value (the critical Richardson number, R_c) of about 0.2. This establishes a limit for mixing length in stratified flow: $\lambda \leq R_c \kappa L$, and it is assumed that in the pycnocline this limit is approached, where L is based on pycnocline fluxes of momentum and buoyancy.

Estimates of mixing length in a near neutral UBL 0018
from the Ice Station Weddell data (**Figure 1**) are illustrated in **Figure 3(A)**. Points marked λ_{peak} were taken from the inverse of the wavenumber at the

peak in the vertical velocity spectra (averaged over all 1-h flow realizations), as described above. Values marked λ_ε were obtained using eqn [8] assuming negligible buoyancy flux, with measured values for u_* and ε (obtained from spectral levels in the inertial subrange). They show clearly that the 'wall layer' scaling, $\lambda = \kappa|z|$ does not hold for depths greater than about 4 m.

0019 Rapid melting reduces the extent of the surface layer and the maximum mixing length (**Figure 2B**). The stability factor $\eta_* = (1 + \Lambda_* u_* / (\kappa R_c |f| L))^{-1/2}$ derives from similarity theory and ensures that the mixing length varies smoothly from the neutral limit ($\lambda_{\max} \to \Lambda_* u_{*0}/|f|$) to the stable limit ($\lambda_{\max} \to \kappa R_c L_0$) for increasing stability. A consequence of reduced scales during melting is formation of a seasonal pycnocline, above a 'trapped' layer with properties indicative of the mixed layer that existed before the freshwater influx.

0020 Rapid ice growth produces negative buoyancy via enhanced salinity at the interface, increasing TKE by the buoyancy production term in eqn [8]. The result is that mixing length and eddy viscosity increase in the UBL, sometimes dramatically. During the 1992 Lead Experiment, turbulent flux and dissipation measured from the edge of a freezing lead in a forced convective regime showed that, compared with the neutral UBL, there was a tenfold increase in mixing length (based on w spectral peaks) and in eddy heat and salt diffusivity (based on measured fluxes and gradients). The Obukhov length was -12 m, about 40% of the mixed layer extent, indicating relatively mild convection, yet the turbulence was greatly altered, apparently by the generation of quasi-organized roll structures in the lead, reminiscent of Langmuir circulations (a thin ice cover precluded any surface waves at the time of the measurements). Mixing length inferred from the lead measurements increased away from the surface following Monin–Obukhov similarity (adapted from atmospheric boundary layer studies), reaching a maximum value roughly comparable to the pycnocline depth scaled by von Kármán's constant.

0021 The density profiles in **Figure 2(B) and (C)** are drawn schematically with slight gradients in the so-called mixed layer. This is at odds with conceptual models of the upper ocean which treat the boundary layer as completely mixed, but is consistent with measurements in the UBL. Wherever scalar fluxes of temperature and salinity are measurable, vertical gradients (albeit small) of mean temperature and salinity are found in the fully turbulent UBL, including statically unstable profiles as in **Figure 2(C)**.

Effective Eddy Viscosity and Diffusivity

Figure 3(C) illustrates different methods for estimating bulk eddy viscosity in the UBL. The distribution labeled K_{SIM} is from the similarity model used to construct the stress profile of **Figure 1(B)** by matching observed stress at 4 m. The vertical distribution labeled K_{local} is the product $\lambda_{\mathrm{peak}} u_*$ at each level (**Figure 3A and B**). Its vertical average value is $0.019\,\mathrm{m^2\,s^{-1}}$. Finally, the dashed line labeled K_{fit} in **Figure 3(B)** is from the least-squares fitted extinction coefficient ($\mathrm{Re}\{\hat{\delta}\}$) for the Ekman stress solution eqn [2]. The last method is sensitive to small stress values at depth: if the bottommost cluster is ignored, $K_{\mathrm{fit}} = 0.020\,\mathrm{m^2\,s^{-1}}$. 0022

The mixing length hypothesis holds for scalar properties of the UBL as well as momentum, so that it is reasonable to express, e.g., kinematic heat flux as 0023

$$\langle w'T' \rangle = -u_* \lambda_T \frac{\partial T}{\partial z} = -K_{\mathrm{H}} \frac{\partial T}{\partial z} \qquad [10]$$

In flows where turbulence is fully developed with large eddies and a broad inertial subrange, scalar eddy diffusivity and eddy viscosity are comparable (*Reynold's analogy*). In stratified flows with internal wave activity and relatively low turbulence levels, momentum may be transferred by pressure forces that have no analog in scalar conservation equations, hence scalar mixing length may be considerably less than λ.

By measuring turbulent heat flux and the mean thermal gradient, it is possible to derive an independent estimate of eddy diffusivity in the UBL from eqn [10]. An example of this method is shown in **Figure 4**, where heat flux measurements averaged over five instrument clusters are compared with the negative thermal gradient. The data are from the same Ice Station Weddell storm as the other turbulence measurements of **Figures 1** and **3**. The mean thermal diffusivity, $K_{\mathrm{H}} = 0.018\,\mathrm{m^2\,s^{-1}}$, is similar to the eddy viscosity (**Figure 3C**). Close correspondence between eddy viscosity and heat diffusivity was also found during the 1989 CEAREX drift north of Fram Strait, and during the 1992 LEADEX project. In the forced convective regime of the latter, salinity flux was measured for the first time, with comparably large values for eddy salt diffusivity as for eddy viscosity and heat diffusivity (but with low statistical significance for the regression of $\langle w'S' \rangle$ against $\partial S/\partial z$). 0024

Outstanding Problems

Mixing in the Pycnocline

0025 Understanding of turbulent mixing in highly stratified fluid just below the interface between the well-mixed layer and pycnocline is rudimentary. Many conceptual models assume, for example, that fluid 'entrained' at the interface immediately assumes the properties of the well-mixed layer (i.e., is mixed completely), so that the interface sharpens during storms as it deepens following the mean density gradient. Instead, measurements during severe storms in the Weddell Sea show upward turbulent diffusion of the denser fluid with a 'feathering' of the interface. Depending on how it is defined, the pycnocline depth may thus decrease significantly during extreme mixing events. Where the bulk stability of the mixed layer is low and there is large horizontal variability in pycnocline depth (as in the Weddell Sea), advection of horizontal density gradients may have large impact on mixing, both by changing turbulence scales and by conditioning the water column for equation-of-state related effects like cabbeling and thermobaric instability.

0026 Even with the advantage of the stable ice platform, observations in the upper pycnocline are hampered by the small turbulence scales, by the difficulty of separating turbulence from high frequency internal wave velocities, and by rapid migration of the interface in response to internal waves or horizontal advection.

Convection in the Presence of Sea Ice

0027 The cold, saline water that fills most of the abyssal world ocean originates from deep convection at high latitudes. Sea ice formation is a (geophysically) very efficient distillation process and may play a critical role in deep convection in areas like the Greenland, Labrador, and Weddell Seas where the bulk stability of the water column is low. By the same token, melting sea ice is a strong surface stabilizing influence that can rapidly shut down surface driven convection as soon as warm water reaches the well mixed layer from below.

0028 Understanding the physics of turbulent transfer in highly convective regimes is a difficult problem both from theoretical and observational standpoints, complicated not only by uncertainty about how large-scale eddies interact with the stably stratified pycnocline fluid, but also by the possibility of frazil ice, small crystals that form within the water column. Depending on where it nucleates, frazil can represent a distributed internal source of buoyancy and heat in the UBL.

0029 Zones of intense freezing tend to be highly heterogeneous, concentrated in lead systems or near the ice margins, and require specialized equipment for studying horizontal structure. Measuring difficulties increase greatly in the presence of frazil ice or supercooled water, because any intrusive instruments present attractive nucleation sites.

0030 In addition to questions of UBL turbulence and surface buoyancy flux, factors related to nonlinearities in the equation of state for sea water may have profound influence on deep convection triggered initially by ice growth and UBL convection. Recent studies have shown, for example, that certain regions of the Weddell Sea are susceptible to *thermobaric instability*, arising from nonlinearity of the thermal expansion coefficient with increasing pressure. The importance of thermobaric instability for an ice-covered ocean is that once triggered, the potential energy released and converted in to turbulence as the water column overturns thermobarically, may be sufficient to override the surface buoyancy flux that would result from rapid melting as warm water reaches the surface.

Symbols

f	Coriolis parameter
g	acceleration of gravity
K	eddy viscosity
K_H	scalar eddy diffusivity
i	imaginary number
L	Obukhov length, $u_*^3/(\kappa\langle w'b'\rangle)$
P_b	production rate of turbulent kinetic energy by buoyancy, $-\langle w'b'\rangle$
P_S	production rate of turbulent kinetic energy by shear, u_*^3/λ
q	turbulent kinetic energy scale velocity
R_c	critical flux Richardson number (~ 0.2)
S	salinity
T	temperature
$\boldsymbol{u}$	three-dimensional velocity vector (u, v, w components)
u_*	friction velocity, square root of kinematic stress
u_τ	turbulence scale velocity
$\boldsymbol{V}$	horizontal velocity vector
w_*	convective turbulence scale velocity
$\langle w'b'\rangle$	turbulent buoyancy flux, $(g/\rho)\langle w'p'\rangle$
$\langle w'T'\rangle$	kinematic turbulent heat flux
$\langle w'S'\rangle$	turbulent salinity flux
$\hat{\delta}$	complex attenuation coefficient: $\sqrt{\lvert f\rvert/(2K)}(1 \pm i)$
ε	dissipation rate of turbulent kinetic energy
η_*	stability factor, $(1 + \Lambda_* u_*/(\kappa R_c \lvert f\rvert L))^{-1/2}$
κ	von Kàrmàn's constant (0.4)

Λ_*	similarity constant (~ 0.03)
λ	turbulent mixing length scale
λ_T	turbulent scalar mixing length scale
ν	kinematic molecular viscosity, units $m^2\,s^{-1}$
ν_T	molecular scalar (thermal) diffusivity, units $m^2\,s^{-1}$
$\hat{\tau}$	Reynolds stress: $\langle u'w' \rangle + i\langle v'w' \rangle$
Φ	latitude

See also

0031 **Arctic Basin Circulation (372). Bottom Water Formation (6). Deep Convection (113). Ice–Ocean Interaction (3). Internal Tides (125). Langmuir Circulation and Instability (141). Wind and Buoyancy-forced Upper Ocean (157).**

Further Reading

Ekman VW (1905) On the influence of the earth's rotation on ocean currents. *Ark. Mat. Astr. Fys.* 2: 1–52.

Gill AE (1982) *Atmosphere–Ocean Dynamics*. New York: Academic Press.

Johannessen OM, Muench RD and Overland JE (eds.) (1994) *The Polar Oceans and Their Role in Shaping the Global Environment: The Nansen Centennial Volume*. Washington DC: American Geophysical Society.

McPhee MG (1994) On the turbulent mixing length in the oceanic boundary layer. *Journal of Physical Oceanography* 24: 2014–2031.

Pritchard RS (ed.) (1980) *Sea Ice Processes and Models*. Seattle, WA: University of Washington Press.

Smith WO (ed.) (1990) *Polar Oceanography. San Diego, CA: Academic Press*.

Untersteiner N (ed.) (1986) *The Geophysics of Sea Ice*. New York: Plenum Press.

[1] Ekman suggested that the 'depth of frictional influence' $D = \pi\sqrt{(2K/f)}$ varied as wind speed divided by $\sqrt{\sin \Phi}$, where Φ is latitude. This implies no f dependence for K. At high latitudes, this has minor impact. a0146fn0001

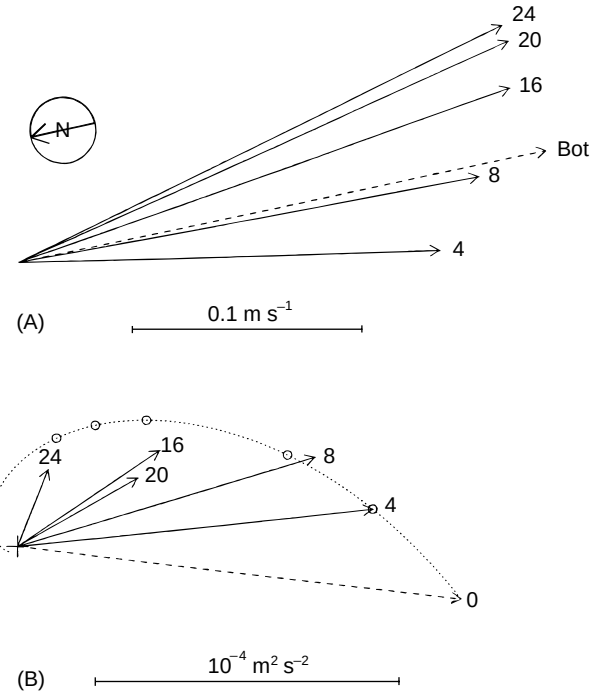

a0146fig0001 **Figure 1** (A) Plan view of mean velocity averaged over a period of steady drift at Ice Station Weddell (1992). Numbers indicate meters from the ice–ocean interface. The vector labeled 'Bot' is the apparent velocity of the seafloor in the drifting reference frame. (B) Horizontal Reynolds stress. The dotted stress hodograph is from a similarity model, with boundary stress (dashed vector) inferred from the model solution that matches observed stress at 4 m. (Reproduced from McPhee MG and Martinson DG (1994) *Science* 263: 218–221.)

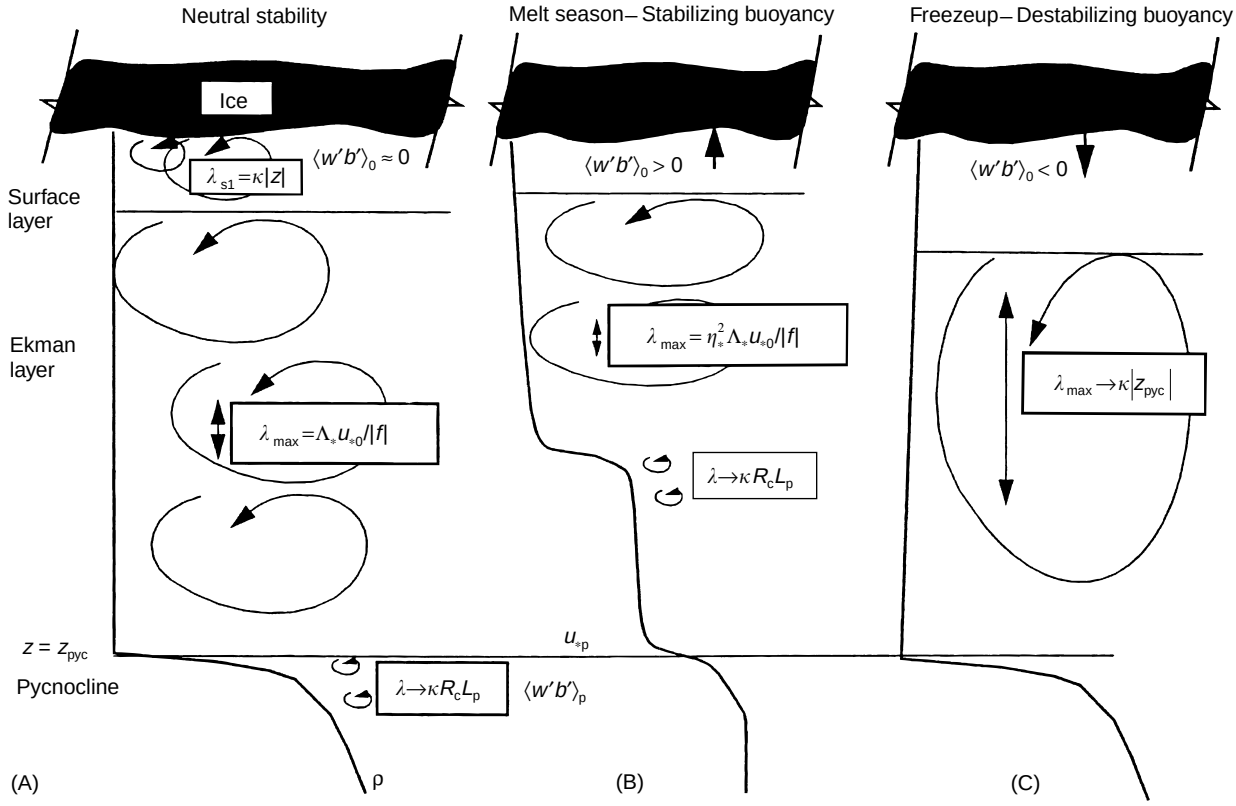

a0146fig0002 **Figure 2** Schematic diagram of mixing length distributions in the UBL under conditions of (A) dynamically negligible surface buoyancy flux (neutral stratification in the well mixed layer), (B) upward buoyancy flux from summer melting, with formation of a seasonal pycnocline and a negative density gradient in the 'well mixed' layer, and (C) downward buoyancy flux from rapid freezing, with positive density gradient to the pycnocline. u_*, Friction velocity; $\langle w'b'\rangle$, buoyancy flux; κ, Kármán's constant, 0.4; Λ_*, similarity constant, 0.028; R_c, critical flux Richardson numbers, 0.2; f, Coriolis parameter; $L = u_*^3/(\kappa\langle w'b'\rangle)$, Obukhov length; $\eta_* = (1 + \Lambda_* u_*/\kappa R_c|f|L))^{-1/2}$.

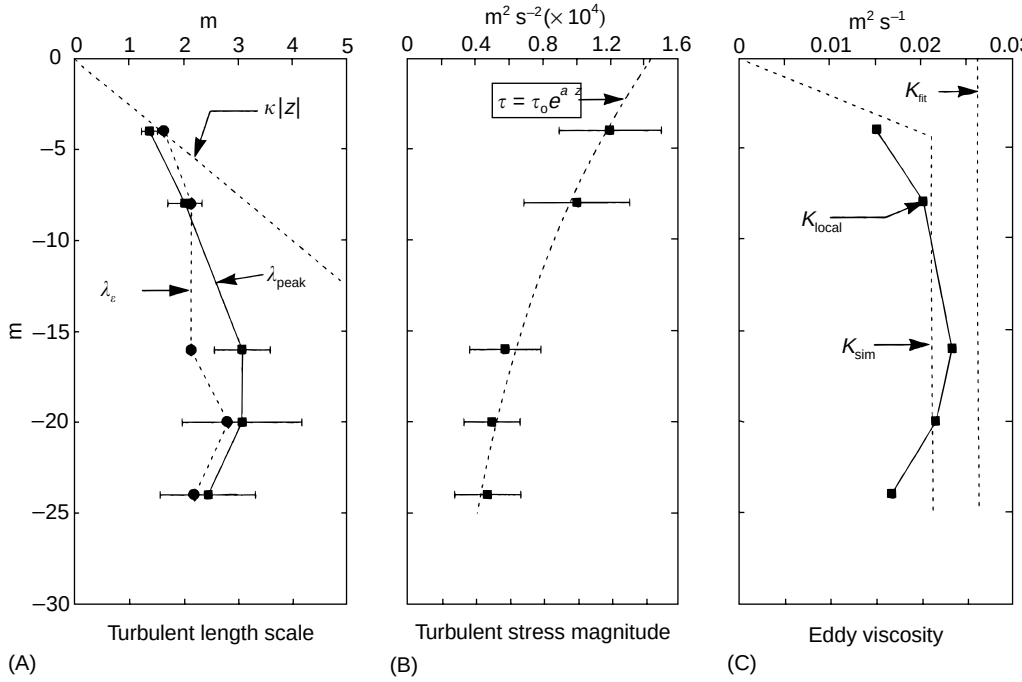

a0146fig0003 **Figure 3** (A) Mixing length determined from the TKE equation (λ_ε) and from the inverse of the wavenumber at the peak in the weighted w spectrum (λ_{peak}). Error bars indicate twice the standard deviation from the spectra calculated from 1-h segments of data. (B) Average Reynolds stress magnitude, with a least-squares fitted exponential decay with depth. Fit coefficients are $\tau_0 = 1.44 \times 10^{-4}\,m^2\,s^{-2}$ and $a = 0.051\,m^{-1}$. (C) Eddy viscosity estimated by three methods as described in the text. (Reproduced from McPhee MG and Martinson DG (1994) *Science* 263, 218–221.)

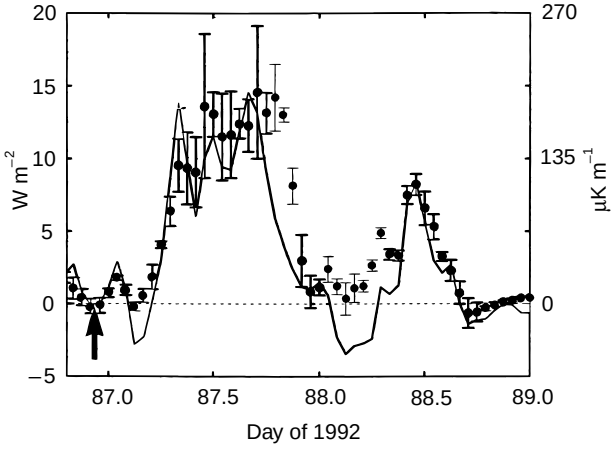

a0146fig0004 **Figure 4** Time series of turbulent heat flux, $\rho c_p \overline{\langle w'T' \rangle}$ (W m^{-2}, circles) and temperature gradient $\partial T/\partial z$ (μK m^{-1} curve). The overbar indicates a vertical average over five turbulence clusters from 4 to 24 m. Error bars are twice the sample standard deviation. The temperature gradient was calculated by linear regression, after the calibration of each thermometer was adjusted by a constant amount so that the gradient was zero at time 86.95 when heat flux was zero (heavy arrow). (Reproduced from McPhee MG and Martinson DG (1994) *Science* 263: 218–221.